Title: Chemoproteomics uncovers widespread medium-chain acylation as a novel protein modification

Authors: Xin Gong[1,2,3], Yanwen Feng[2,3], Xue Bai[1], Jin Hu[1], Shan Feng[1], Ling Yang[1], Hongyun Tang[1,2,3,4]*

[1] State Key Laboratory of Gene Expression, School of Life Sciences, Westlake University, Hangzhou 310024, China

[2] Westlake Laboratory of Life Sciences and Biomedicine, Hangzhou 310024, China

[3] Institute of Biology, Westlake Institute for Advanced Study, Hangzhou 310024, Zhejiang, China

[4] Lead contact

*Correspondence: tanghongyun@westlake.edu.cn

Abstract

While medium-chain fatty acids (MCFAs; C6-C12) are key metabolites with profound physiological roles, their potential to covalently modify proteins remains an open question, with octanoylation of only one protein documented to date. Here, we report the discovery of three novel MCFA modifications, including hexanoylation (C6), decanoylation (C10), and dodecanoylation (C12), and present the first proteome-wide analysis of medium-chain acylation. Using chemo-proteomic methods, we identified hundreds of protein substrates for each modification, including 270 hexanoylated, 131 octanoylated, 286 decanoylated, and 509 dodecanoylated proteins. We further validated cysteine hexanoylation by mass spectrometry in FAHD2A, a mitochondrial oxaloacetate isomerase highly enriched among the 270 hexanoylated proteins, and identified the putative “writer” and “eraser” enzymes, acyltransferase ZDHHC3 and deacylase SIRT4, respectively. Our discovery of medium-chain acylation significantly expands the landscape of protein lipidation, and the proteomic atlas of medium-chain acylation provides a foundational resource for elucidating the mechanisms underlying the MCFA’s physiological functions.

Keywords: Medium-chain acylation; Hexanoylation; Octanoylation; Decanoylation; Dodecanoylation; FAHD2A; ZDHHC3; SIRT4

Introduction

Medium-chain fatty acids (MCFAs), lipids composed of 6 to 12 carbon atoms, are important bioactive metabolites with significant physiological roles and health benefits[1-4]. Distinguished from their long-chain counterparts, MCFAs are rapidly absorbed and transported directly to the liver, where they efficiently enter mitochondria for β-oxidation without reliance on the carnitine shuttle system[2,5,6]. This unique metabolic feature allows them to powerfully influence energy homeostasis, ketogenesis, and cellular signaling pathways, making them promising therapeutic agents for conditions such as diabetes and epilepsy[3,4,7,8]. Despite their important functions, the molecular mechanisms underlying MCFAs activity remain poorly understood, particularly their capacity to regulate protein function. A fundamental unresolved question is whether MCFAs act as signaling molecules through covalently modifying proteins, which has remained largely unexplored.

Protein acylation is an important mechanism by which fatty acids modulate protein function and represents a critical post-translational modification (PTM) that regulates protein stability, localization, and activity, with well-established implications in health and disease[9-11]. The landscapes of long-chain (e.g., palmitoylation) and short-chain (e.g., lactylation) acylations are well characterized. For instance, S-palmitoylation, which governs membrane targeting and protein–protein interactions, occurs on hundreds of proteins and is essential for various physiological activities, such as immune recognition, cell differentiation, and signal transduction[12-14]. Similarly, short-chain acylations such as lactylation regulate diverse biological processes, including epigenetic regulation, tumorigenesis, and innate immunity[15-19]. In stark contrast, medium-chain acylation is represented by only one known example: the O-octanoylation of ghrelin, the “hunger hormone,” catalyzed by the enzyme ghrelin O-acyltransferase (GOAT)[20-22]. This striking gap prompts us to explore the existence of a broader, uncharacterized family of MCFA-driven protein modifications, including hexanoylation, decanoylation, and dodecanoylation.

Here, we combine metabolic labeling with chemoproteomic approaches to report the discovery of these three novel medium-chain acylations. We present the first proteome-wide analysis of all types of even-numbered medium-chain acylations, identifying comprehensive sets of protein substrates for each modification. Focusing on hexanoylation, we validate modification sites on the mitochondrial protein FAHD2A at Cys215 and Cys301 and identify the putative

"writer" and "eraser" enzymes—acyltransferase ZDHHC3 and deacylase SIRT4. Collectively, these findings establish medium-chain acylation as a widespread post-translational modification, providing a foundational resource for future investigations into the regulatory roles of MCFAs in various biological processes.

Results

A chemoproteomic strategy reveals widespread medium-chain acylations

To test the hypothesis that a family of medium-chain acylations extends beyond octanoylation, we employed metabolic labeling using azide analogs of hexanoic (C6), octanoic (C8), decanoic (C10), and dodecanoic (C12) acids (Fig. 1a). To evaluate overall levels of medium-chain acylations, HepG2 cells were treated with each azide MCFA probe, and cell lysates were subsequently subjected to click chemistry conjugation with biotin-alkyne to label azide MCFA probe-modified proteins (Fig. 1b). This approach revealed a significant, probe-dependent increase in biotin signal relative to DMSO controls, providing evidence for the widespread existence of protein hexanoylation, octanoylation, decanoylation, and dodecanoylation (Fig. 1c).

Next, we conducted the first proteome-wide profiling of medium-chain acylations. Using an optimized enrichment workflow that involves covalently linking acylated proteins onto alkyne-agarose beads, enabling highly efficient removal of nonspecific binding and background noise (Fig. 1d), we identified comprehensive sets of substrates for each of these four medium-chain acyl modifications. This analysis revealed 270 hexanoylated, 131 octanoylated, 286 decanoylated, and 509 dodecanoylated proteins, establishing medium-chain acylation as a prevalent post-translational modification (Fig. 1e-h and Tables 1–4).

Our Gene Ontology (GO) enrichment analysis revealed distinct functional associations across the acylomes. In terms of biological processes, hexanoylated, octanoylated, decanoylated and dodecanoylated proteins were all enriched in metabolic processes, such as small molecule catabolic process and fatty acid metabolic process (Extended Data Fig. 1a-d), implying the role of medium-chain fatty acylation in modulating metabolism. Regarding cellular components, octanoylated proteins were enriched in focal adhesion (Fig. 1j), decanoylated proteins were enriched in lysosomal membrane (Fig. 1k), and dodecanoylated proteins were enriched in secretory granule membrane (Fig. 1l). Notably, the hexanoylome exhibited a striking and unique enrichment for mitochondrial proteins, with more than one-third (93 of 270) localized to

mitochondria (Fig. 1i), implicating protein hexanoylation as a crucial, previously unrecognized regulator of mitochondrial functions. Given this specific subcellular and functional enrichment, our subsequent studies focused on validating and mechanistically characterizing protein hexanoylation.

Validation of hexanoylation in FAHD2A

To rigorously validate protein hexanoylation, we focused on FAHD2A, a mitochondrial oxaloacetate hydrolase[23] and a top hit from our proteomic screen. High-resolution mass spectrometry of FAHD2A purified from HepG2 cells identified two peptides (KGDEVQC$_{hex}$EIEELGVIINK and TFDTFC$_{hex}$PLGPALVTK) with a +98.0726 Da mass shift on cysteine residues (Cys215 and Cys301), consistent with the presence of hexanoylation (Fig. 2a and Extended Data Fig. 2a, labeled "endogenous"). To confirm this modification, we performed HPLC-tandem mass spectrometry (MS/MS) analyses, comparing endogenous FAHD2A-derived peptides with their *in vitro* synthesized hexanoylated counterparts and corresponding mixtures. We found that their fragmentation patterns were identical (Fig. 2a–b and Extended Data Fig. 2a), unambiguously assigning hexanoylation to Cys215 and Cys301.

We further validated the existence of hexanoylation through multiple independent approaches. First, we confirmed the hexanoylation of FAHD2A in both HepG2 and 293T cells expressing FAHD2A-FLAG by metabolic labeling with azido-hexanoic acid, followed by anti-FLAG immunoprecipitation of FAHD2A-FLAG, click chemistry-mediated conjugation to alkyne-biotin, and detection using anti-biotin antibody (Fig. 2c, 2d). This result also supports the generality of protein hexanoylation across different cells. Importantly, we performed site-directed mutagenesis replacing Cys301 with serine (C301S) and demonstrated that the C301S mutation markedly reduced FAHD2A hexanoylation, confirming Cys301 as a key site of hexanoylation modification (Fig. 2e, 2f). Crucially, metabolic labeling with deuterium-labeled D11-hexanoic acid resulted in a corresponding +109.1422 Da mass shift in FAHD2A peptides bearing Cys215 hexanoylation (Extended Data Fig. 2b, 2c), confirming that the hexanoylation can be directly derived from the exogenous fatty acid and thereby supporting that hexanoylation is responsive to the changes in hexanoic acids. Together, these data demonstrate the existence of cysteine hexanoylation.

The acyltransferase ZDHHC3 is a putative "writer" of protein hexanoylation

We next sought to identify the enzymes responsible for catalyzing protein hexanoylation. Given the occurrence of protein hexanoylation at cysteine residues, we hypothesized that members of the ZDHHC family of protein acyltransferases, which catalyze thioester bond formation[12,14,24], may act as the "writers" of protein hexanoylation. Indeed, we found that in HepG2 cells expressing FAHD2A-FLAG, overexpression of ZDHHC3 robustly increased the hexanoylation of FAHD2A-FLAG by approximately 1.5-fold (Fig. 3a, 3b). To assess the endogenous requirement of ZDHHC3 for hexanoylation, we employed shRNA-mediated knockdown to decrease ZDHHC3 expression in HepG2 cells (Extended Data Fig. 3a). Consitent with a role of ZDHHC3 in promoting hexanoylaiton, decrease of ZDHHC3 reduced FAHD2A hexanoylation by approximately 50% (Fig. 3c, 3d). Subsequently, we determined that ZDHHC3 functions as a broad-spectrum regulator of the cellular hexanoylome. Over-expression of ZDHHC3 robustly amplified global protein hexanoylation signals (Fig. 3e), whereas its depletion resulted in a profound attenuation of these modifications (Fig. 3f). Given that many hexanoylated proteins, including FAHD2A, are localized to mitochondria, we examined a potential mitochondrial distribution of ZDHHC3. Surprisingly, immunofluorescence analysis revealed that ZDHHC3 did not colocalize with MitoTracker-stained mitochondria (Extended Data Fig. 3b), implying that it may mediate hexanoylation in the cytosol prior to the mitochondrial import of substrate proteins. Together, these results support ZDHHC3 as a putative hexanoyl-acyltransferase.

The deacylase SIRT4 acts as a potential "eraser" of protein hexanoylation

The reversibility of protein modification is critical for their regulatory function[12,25,26]. To identify the enzymes responsible for removing hexanoylation, we screened broad-spectrum inhibitors of the two major deacylase families, histone deacetylases (HDACs) and sirtuins (SIRTs)[27,28]. Treatment with the sirtuin inhibitor nicotinamide (NAM), but not the HDAC inhibitor trichostatin A (TSA), significantly increased FAHD2A hexanoylation by >2 fold, implicating a sirtuin as the putative "eraser" (Fig. 4a, 4b).

We then screened all seven SIRT members for their ability to dehexanoylate FAHD2A. We first performed subcellular localization analyses of these SIRT proteins, and found that SIRT3, SIRT4, and SIRT5 show strong mitochondrial localization as showing by their colocalization with MitoTracker staining (Extended Data Fig. 4a). In light of the widespread occurrence of mitochondrial hexanoylation, we investigated the potential involvement of those three

mitochondrial sirtuins. Among these three, overexpression of SIRT4 caused the most potent reduction in FAHD2A hexanoylation levels, decreasing levels to approximately 30% of those observed in the control (Fig. 4c, 4d). Reversely, knockdown of endogenous SIRT4 (Extended Data Fig. 4b) resulted in an approximately twofold increase in FAHD2A hexanoylation (Fig. 4e, 4f), further supporting that SIRT4 is likely an endogenous dehexanoylase for FAHD2A. Furthermore, we investigated whether SIRT4 regulates hexanoylation globally. Overexpression of SIRT4 significantly reduced overall cellular protein hexanoylation (Fig. 4g), whereas SIRT4 knockdown resulted in an increase in global hexanoylation (Fig. 4h). Collectively, these findings identify SIRT4 as a possible dehexanoylase, providing a dynamic and reversible regulatory mechanism for protein hexanoylation.

Discussion

Medium-chain fatty acids have long been appreciated as unique metabolic fuels, but their role as direct regulators has remained a significant blind spot[3]. Our study demonstrates that MCFAs are precursors for a widespread and dynamic family of protein post-translational modifications. We report the discovery of three novel protein acylations, including hexanoylation, decanoylation, and dodecanoylation, and provide the first proteome-wide maps of all even-numbered medium-chain fatty acid acylations. Focusing on hexanoylation, we not only validate this modification on the mitochondrial protein FAHD2A but also identify the possible "writer," acyltransferase ZDHHC3, and "eraser," the deacylase SIRT4. These findings reveal medium-chain acylation and offer a comprehensive atlas of such modifications, establishing a foundational resource for elucidating the regulatory functions of MCFAs.

Our identification of ZDHHC3 as a putative hexanoyltransferase expands the known substrate scope of the ZDHHC family. While these enzymes are canonical protein palmitoyltransferases (C16)[29-31], our data support that ZDHHC3 may also efficiently utilize hexanoyl-CoA, a significantly shorter acyl-CoA substrate. This functional plasticity suggests that different ZDHHC enzymes may have distinct acyl-CoA preferences, enabling them to respond to specific metabolic cues and generate diverse acyl-proteomes. The discovery of ZDHHC3's role in hexanoylation provides a critical tool for future studies aimed at dissecting the function of this modification through genetic manipulation of its writer. Moreover, our discovery adds a new enzymatic activity

to the multi-functional repertoire of SIRT4, which is already known to possess deacetylase[32], ADP-ribosyltransferase[33], and lipoamidase activities[34]. The regulatory mechanisms by which SIRT4 coordinates the removal of these diverse post-translational modifications, including hexanoylation, remains to be determined. Given that hexanoylation is sensitive to changes in hexanoic acid levels, it is crucial to investigate how ZDHHC3 and SIRT4 respond to fluctuations in medium-chain fatty acid concentrations, both in dietary intake and within the organism.

This study lays a foundational groundwork, but it also opens up numerous avenues for future investigation. While we have identified the writer/eraser pair for hexanoylation, the enzymes governing decanoylation and dodecanoylation remain to be discovered. Furthermore, the functional consequence of hexanoylation on FAHD2A and the other 269 target proteins is a critical next question. Does this PTM alter enzymatic activity, protein stability, or protein-protein interactions within mitochondria? Given the special roles of MCFAs in modulating diseases like ketosis and diabetes, elucidating these functional outcomes will be essential for connecting this new regulatory layer to these physiological states. In conclusion, our work identifies medium-chain fatty acids as important modifiers of proteins, and by mapping the proteome of this newly characterized class of acylations and elucidating the enzymatic machinery governing their dynamics, we provide a framework for understanding mechanisms by which medium-chain fatty acids directly regulate protein function.

Materials and Methods

Cell culture and treatments

HEK293T (ATCC, CRL-3216) and HepG2 (ATCC, HB-8065) cells were maintained in Dulbecco's Modified Eagle Medium (DMEM; Sigma, D6429) supplemented with 10% fetal bovine serum (FBS; ExCell, FSP500) and 1% Penicillin-Streptomycin (Yeasen, 60162ES76). All cells were cultured at 37°C in a humidified incubator with 5% CO_2 and routinely tested for mycoplasma contamination. For treatments, the following reagents were used as indicated in the figure legends: trichostatin A (TSA; MCE, HY-15144) at a final concentration of 3 μM for 48 h, nicotinamide (NAM; MCE, HY-B0150) at a final concentration of 5 mM for 48 h, azido-hexanoic acid (Click Chemistry Tools, 1250) at a final concentration of 100 μM for 48 h, azido-octanoic acid (Amatek Scientific, AC-8025) at a final concentration of 100 μM for 48 h, azido-decanoic

acid (Amatek Scientific, AS00787) at a final concentration of 100 μM for 48 h, azido-dodecanoic acid (Amatek Scientific, AS00792) at a final concentration of 100 μM for 48 h, D11-hexanoic acid (Cambridge Isotope Laboratories, DLM-277-PK) at a final concentration of 500 μM for 48 h, and dimethyl sulfoxide (DMSO; Sigma, 4540) as a vehicle control.

Reagents and antibodies

The reagents and antibodies used in this study were as follows: Trypsin 0.25% EDTA (Thermo Fisher, 25200072), BSA (GENVIEW, FA016), ExpressPlusTM PAGE Gels (GenScript, M42010C), Coomassie Blue Destaining Buffer (GenStar, E155-01), Protein marker (Cofitt, LBP6510), XbaI (NEB, R0145S), BamHI (NEB, R3136), AgeI (NEB, R3552S), EcoRI (NEB, R3101L), XhoI (NEB, R0146S), Q5 enzyme (NEB, M0543L), ClonExpress Ultra One Step Cloning kit (Vazyme, C115), KOD-Plus-Mutagenesis Kit (Toyobo, SMK-101), anti-SIRT4 antibody (Proteintech, 66543-1-Ig, 1:1000 dilution), anti-FAHD2A (Sigma, HPA44987, 1:1000 dilution), anti-COX IV (HuaBio, ET1701-63, 1:1000 dilution), anti-Biotin antibody (Cell Singaling Technology, 7075S), anti-FLAG antibody (HuaBio, M1403-2, 1:1000 dilution), anti-β-Actin antibody (ABclonal, AC026, 1:2000 dilution), anti-HRP Conjugated Goat anti-Rabbit IgG (HuaBio, HA1001, 1:10000 dilution), and anti-HRP Conjugated Goat anti-Mouse IgG (HuaBio, HA1006, 1:10000 dilution). For shRNA transfection vectors, shRNA vectors to knock down endogenous ZDHHC3 were obtained from Sigma (TRCN0000133710, TRCN0000159818, or TRCN0000164379) and shRNA vectors to knock down endogenous SIRT4 were obtained from Sigma (TRCN0000232894).

Lentivirus Production and Transduction (Spinfection)

Lentiviral particles were produced by transient transfection of HEK293T cells. Cells were seeded in 6-well plates at a density of 5 x 10^5 cells/well. The following day, cells were co-transfected with 1 μg of the target lentiviral vector along with the packaging plasmids pMD2.G (1 μg) and psPAX2 (1 μg), using Lipofectamine 8000 (Beyotime, C0533) in Opti-MEM medium (Thermo Fisher, 51985034) according to the manufacturer's protocol. Virus-containing supernatants were harvested 48 hours post-transfection, centrifuged at 300 x g for 5 minutes to remove cell debris, and filtered through a 0.45 μm PES membrane. Aliquots were stored at -80°C until use.

For transduction, HepG2 cells were seeded at a density of 1 x 10^6 cells/well in a 6-well plate and allowed to adhere overnight. On the day of infection, the culture medium was replaced with fresh DMEM containing 10 μg/mL polybrene (Beyotime, C0351). An appropriate volume of lentiviral supernatant was added to each well. The plate was then centrifuged at 700 x g for 30 minutes at 30°C to facilitate infection, a process known as 'spinfection'. Following centrifugation, cells were incubated at 37°C for 48 hours. After this period, transduced cells were selected and expanded using puromycin (Gibco, A113803) at 5 μg/mL or G418 (Beyotime, ST081) at 50 μg/mL for at least 4 days before use in subsequent experiments.

Click chemistry for medium-chain acylation detection

Metabolic labeling and cell lysis: HepG2 cells were metabolically labeled for 48 hours with 100 μM of the indicated azido-MCFA probe or with DMSO as a vehicle control. Following labeling, cells were washed with cold PBS and harvested. After being collected by centrifugation (300 g, 5 min, 4°C), the cells were lysed on ice for 10 min in lysis buffer (20 mM Tris-HCl pH 7.5, 150 mM NaCl, 1% Triton X-100, 1 × protease inhibitor cocktail (Sigma, P8340). To ensure complete lysis, the samples were sonicated on ice (35% amplitude, 3 s on / 4 s off, for a total of 1 min sonication time). Insoluble cellular debris was removed by centrifugation at 12,000 g for 10 min at 4°C. The cleared supernatant was collected, and the protein concentration was determined using a BCA assay (GenStar, E162-01).

In-lysate click reaction with alkyne-biotin: The click chemistry reaction was performed on 200 μg of protein lysate. The reaction was assembled with the following components added sequentially: lysate, alkyne-biotin (final concentration 40 μM) (Click Chemistry Tools, CCT-TA105), a copper(I)-stabilizing ligand THPTA (Sigma, 762342), copper(II) sulfate (final concentration 1-2 mM) (Sigma, 209198), and freshly prepared sodium L-ascorbate (final concentration 5 mM) (Sigma, A7631). The reaction was incubated for 30 minutes at room temperature in the dark.

Protein precipitation and sample preparation for Western blot: Following the click reaction, proteins were precipitated using a standard methanol/chloroform method[35]. Briefly, 600 μL of methanol, 150 μL of chloroform, and 400 μL of water were added sequentially with vortexing. The mixture was centrifuged at 15,000 x g for 5 min, and the protein pellet at the interface was collected. The pellet was washed twice with cold methanol, briefly air-dried, and resuspended in

100 µL of Tris-HCl buffer (50 mM, pH 7.4) containing 1% SDS. Complete resuspension was achieved by heating at 70°C for 20 min. The protein concentration was re-quantified to ensure equal loading. For analysis, 20 µg of protein per sample was mixed with 5x SDS-PAGE Plus loading buffer (Genstar, E151-10), heated at 70°C for 10 min, and resolved by SDS-PAGE for subsequent immunoblotting.

RNA extraction and qPCR analysis

Total RNA was isolated using the RNA isolation kit (Qmega, R6831) according to the manufacturer's protocol. cDNA was then generated using EasyScript® One-Step gDNA Removal and cDNA Synthesis SuperMix (TransGen Biotech, AE311-03). qPCR with Luna® Universal qPCR Master Mix (NEB, M3003L) was carried out using Quantitative fluorescent PCR detection system (Jena, Qtower3G). The primer sequences are provided in Supplementary Table 5.

Confocal Microscopy and Live-Cell Staining

HepG2 cells expressing the indicated transgenes were seeded at a density of 1 x 10^5 cells per 20 mm glass-bottom culture dish and allowed to adhere for 24 hours. For live-cell imaging, mitochondria were stained by incubating cells with 200 nM MitoTracker Green (Thermo Fisher, M7514) in culture medium for 30 minutes at 37°C. Following this, nuclei were stained by incubating cells with Hoechst 33342 (1x final concentration from a 100 x stock; Beyotime, C1027) for 10 minutes at 37°C. Between staining steps, cells were washed with pre-warmed culture medium. After the final wash, cells were maintained in fresh culture medium for imaging. Fluorescence images were acquired using a Nikon A1R laser scanning confocal microscope.

Chemoproteomic Enrichment of Medium-Chain Acylated Proteins

Metabolic labeling and cell lysis: HepG2 cells (5 x 10^7 per replicate) were metabolically labeled for 48 hours with either 100 µM of azido-hexanoic acid, azido-octanoic acid, azido-decanoic acid, azido-dodecanoic acid, or DMSO as a vehicle control. Cell pellets were lysed in 1 mL of lysis buffer (Click-&-Go™ Plus Protein Enrichment Kit, Click Chemistry Tools, CCT-1033) by vortexing for 30 min at 4°C. Lysates were cleared by centrifugation at 10,000 x g for 5 min at 4°C. Protein concentration was determined, and approximately 3 mg of total protein was used for each enrichment.

Click chemistry reaction on agarose beads: Alkyne-functionalized agarose beads (200 µL slurry; Click-&-Go™ Plus Protein Enrichment Kit, Click Chemistry Tools, CCT-1033) were washed three times with nuclease-free water. The click reaction was performed by combining the washed beads with 800 µL of cleared lysate, 860 µL of water, 100 µL of Tris-amine buffer (82 mM), 20 µL of $CuSO_4$ (100 mM), and 20 µL of freshly prepared sodium L-ascorbate (80 g/L). The reaction was incubated for 20 h at room temperature with end-over-end rotation, protected from light.

Bead washing, reduction, and alkylation: Following the click reaction, beads were centrifuged (1,000 x g, 1 min) and washed extensively to remove non-specifically bound proteins. The wash sequence was as follows: 3x with Milli-Q water. Beads were then resuspended in 1 mL of Agarose Wash Buffer containing 10 mM DTT and incubated at 70°C for 15 min for reduction. After cooling to room temperature, proteins were alkylated by adding 40 mM iodoacetamide and incubating for 30 min in the dark.

Stringent washes and on-bead digestion: For stringent removal of contaminants, the beads were transferred to spin columns and subjected to a series of high-volume washes: 10x with 2 mL of 1% SDS buffer, 20x with 2 mL of 8 M urea in 100 mM Tris (pH 8.0), and 20x with 2 mL of 20% acetonitrile. For on-bead digestion, the beads were equilibrated with digestion buffer (40 mM NH_4HCO_3, 10% acetonitrile) and resuspended in approximately 200 µL of the same buffer. Trypsin (3 µg; proteomics grade; Promega, V5280) was added, and the digestion was carried out for 14 h at 37°C with gentle agitation.

Peptide recovery and desalting: Tryptic peptides were recovered from the supernatant by centrifugation (1,000 x g, 5 min). The beads were washed three times with 300 µL of water, and all fractions were combined. The combined peptide solution was acidified with trifluoroacetic acid (TFA) to a final concentration of 0.2% and adjusted to 2% acetonitrile. Peptides were then desalted and concentrated using C18 spin columns (Waters, WAT094225) according to standard protocols (methanol activation, water equilibration, sample loading, wash with 5% methanol, and elution with 80% methanol). The eluates were dried completely in a vacuum concentrator (Christ, CT02-50) and stored at -20°C until LC-MS/MS analysis.

Immunoprecipitation of FAHD2A for Click Chemistry Analysis (IP-Click)

HepG2 cells stably expressing FAHD2A-FLAG (3 x 10^7 cells per condition) were treated for 48 h with either 100 µM azido-hexanoic acid or DMSO as a vehicle control. After treatment, cells were harvested, washed once with ice-cold PBS, and lysed in 10 mL of lysis buffer (50 mM Tris-HCl pH 7.5, 150 mM NaCl, supplemented with protease inhibitors) on ice for 10 min. Lysates were sonicated on ice (35% amplitude; 20 cycles of 3 s on / 4 s off) and subsequently cleared by centrifugation at 12,000 g for 10 min at 4°C. The cleared supernatant was used for immunoprecipitation.

200 µL of anti-FLAG M2 magnetic beads (Sigma, M8823) were equilibrated by washing three times with ice-cold TBST (50 mM Tris-HCl pH 7.5, 150 mM NaCl, 0.1% Tween-20). The equilibrated beads were added to the clarified lysate and incubated overnight at 4°C with end-over-end rotation. The following day, the beads were washed extensively (8 times with 1 mL of ice-cold TBST) to remove non-specific binders. Bound FAHD2A-FLAG was eluted by incubating the beads with 100 µL of elution buffer (1x PBS containing 250 µg/mL 3x FLAG peptide; Sigma, A36806) for 30 min at room temperature with gentle agitation. The eluate containing purified FAHD2A-FLAG was collected and used immediately for downstream click chemistry reactions.

LC-MS/MS Analysis of Immunopurified FAHD2A

Immunopurified FAHD2A-FLAG was resolved by SDS-PAGE, and the gel was stained with Coomassie Blue G-250 (GenStar, E154-01). The protein band corresponding to FAHD2A was excised and cut into small pieces. In-gel digestion was performed as follows: the gel pieces were subjected to reduction with 25 mM DTT (Sigma, D9163) and alkylation with 55 mM iodoacetamide (Sigma, I6125), followed by overnight digestion with sequencing-grade trypsin (Promega, V5280) in 50 mM ammonium bicarbonate (NH_4HCO_3, Sigma, 09830) at 37°C. The resulting tryptic peptides were extracted twice from the gel matrix with 0.1% formic acid (FA) in 50% acetonitrile (ACN) aqueous solution. The pooled extracts were then dried in a vacuum concentrator before analyses.

For LC-MS/MS analysis, the peptides were resuspended in 0.1% formic acid and 50% acetonitrile automatically injected using Bruker's nanoElute UHPLC System onto the 25 cm column equipped with emitter (Aurora series, CSI, 25 cm × 75 µm ID, 1.6 µm C18, IonOpticks). Bound peptides were then eluted over 30 min at a constant flow rate of 300 nl/min and the mobile phases water/0.1% FA and ACN/0.1% FA (A and B, respectively) were applied in the linear

gradients starting from 2% B and increasing to 22% in 5 min, followed by an increase to 35% B in 15 min, 55% B in 22 min, 80% B in 26 min, 80% B in 26–30 min. Eluted peptides were sprayed into a TIMS quadrupole time-of-flight instrument (timsTOF Pro 2, Bruker Daltonics) using a nano-electrospray source (CaptiveSpray source, Bruker Daltonics). Samples were measured in dda-PASEF mode and the dda-PASEF windows scheme was ranging in dimension m/z from 300 to 1500 and in dimension 1/K0 0.75–1.3, with Ramp Time 166 ms.

Following data acquisition, raw data files were converted into mgf and processed using Thermo Proteome Discoverer software (v2.5) with the Sequest HT search engine. Searches were performed against a custom database containing only the human FAHD2A protein sequence (obtained from UniProt) to maximize sensitivity for modification detection. The search parameters included a precursor mass tolerance of 10 ppm, a fragment mass tolerance of 0.02 Da, trypsin as the enzyme with up to two missed cleavages allowed, and carbamidomethylation of cysteine as a fixed modification. Variable modifications included oxidation of methionine and hexanoylation of cysteine (+98.0726 Da). The false discovery rate (FDR) was set to < 1% at both the peptide and protein levels. MS/MS spectra for figures were plotted using Origin software.

Statistical Analysis

All statistical analyses were performed using GraphPad Prism (v9.0). Data are presented as mean ± SEM from at least three independent biological replicates, as indicated in the figure legends. Comparisons between two groups were analyzed using a two-tailed unpaired Student's t-test. For comparisons among three or more groups, one-way analysis of variance (ANOVA) was used, followed by an appropriate post-hoc test for multiple comparisons (e.g., Dunnett's test) to determine significance between specific groups. For all experiments, statistical significance was defined as $P < 0.05$, with exact P values provided in the respective figures. To ensure reproducibility, all experiments were conducted for at least three independent replicates.

Acknowledgments

We appreciate the discussion and suggestions from Qi Hu (Westlake Univeristy) and the Tang lab. We are also thankful to the facilities at Westlake University, including the Mass Spectrometry and Metabolomics Core, Laboratory Animal Resources Center, High-Performance Computing

Center, Flow Cytometry Core, and Microscopy Core. This work was supported by the National Natural Science Foundation of China (No. 32530030, No. 32350015, and No. 32070565), the Zhejiang Provincial Natural Science Foundation of China (No. XHD24C0701 and No. LQ23C040002), Westlake Center for Genome Editing program (No. 21200000A992510/004), State Key Laboratory of Gene Expression, the HRHI program (No. 202209003 and No. 202109007) of the Westlake Laboratory of Life Sciences and Biomedicine, and the Westlake Education Foundation of Westlake University.

Author contributions

H. T. conceptualized and supervised the study. H. T. and X. G. designed all experiments. X. G. conducted the majority of the experiments and performed data analysis. Y. F. carried out a subset of assays for the detection of cellular hexanoylation and the enrichment of hexanoylated proteomes. S. F., J. H., and X. B. performed mass spectrometry sample preparation and data acquisition. L. Y. performed proteome data analysis. H. T. and X. G. wrote the manuscript with input from all authors.

Declaration of interests

The authors declare no competing interests.

References

1 Kim, C. H. Short-, medium-, versus long-chain fatty acids: mechanisms of immunomodulation and disease pathogenesis. *Cellular & Molecular Immunology* **23**, 594-606, doi:10.1038/s41423-026-01412-z (2026).

2 Li, J. *et al.* Tubular ACSM3 deficiency impairs medium-chain fatty acid metabolism and aggravates kidney fibrosis. *Proc Natl Acad Sci U S A* **122**, e2505752122, doi:10.1073/pnas.2505752122 (2025).

3 Huang, L., Gao, L. & Chen, C. Role of Medium-Chain Fatty Acids in Healthy Metabolism: A Clinical Perspective. *Trends Endocrinol Metab* **32**, 351-366, doi:10.1016/j.tem.2021.03.002 (2021).

4 Nagao, K. & Yanagita, T. Medium-chain fatty acids: functional lipids for the prevention and treatment of the metabolic syndrome. *Pharmacol Res* **61**, 208-212, doi:10.1016/j.phrs.2009.11.007 (2010).

5 Schonfeld, P. & Wojtczak, L. Short- and medium-chain fatty acids in energy metabolism: the cellular perspective. *J Lipid Res* **57**, 943-954, doi:10.1194/jlr.R067629 (2016).

6 Cao, Y. *et al.* Dietary medium-chain fatty acids reduce hepatic fat accumulation via activation of a CREBH-FGF21 axis. *Mol Metab* **87**, 101991, doi:10.1016/j.molmet.2024.101991 (2024).

7 Dunn, E., Zhang, B., Sahota, V. K. & Augustin, H. Potential benefits of medium chain fatty acids in aging and neurodegenerative disease. *Front Aging Neurosci* **15**, 1230467, doi:10.3389/fnagi.2023.1230467 (2023).

8 Augustin, K. *et al.* Mechanisms of action for the medium-chain triglyceride ketogenic diet in neurological and metabolic disorders. *Lancet Neurol* **17**, 84-93, doi:10.1016/S1474-4422(17)30408-8 (2018).

9 Shang, S., Liu, J. & Hua, F. Protein acylation: mechanisms, biological functions and therapeutic targets. *Signal Transduct Target Ther* **7**, 396, doi:10.1038/s41392-022-01245-y (2022).

10 Wu, X. *et al.* Targeting protein modifications in metabolic diseases: molecular mechanisms and targeted therapies. *Signal Transduct Target Ther* **8**, 220, doi:10.1038/s41392-023-01439-y (2023).

11 Liu, Y. Q., Yang, Q. & He, G. W. Post-translational acylation of proteins in cardiac hypertrophy. *Nat Rev Cardiol* **22**, 944-960, doi:10.1038/s41569-025-01150-1 (2025).

12 Anwar, M. U. & van der Goot, F. G. Refining S-acylation: Structure, regulation, dynamics, and therapeutic implications. *J Cell Biol* **222**, doi:10.1083/jcb.202307103 (2023).

13 Chamberlain, L. H. & Shipston, M. J. The physiology of protein S-acylation. *Physiol Rev* **95**, 341-376, doi:10.1152/physrev.00032.2014 (2015).

14 F, S. M. *et al.* Mechanisms and functions of protein S-acylation. *Nat Rev Mol Cell Biol* **25**, 488-509, doi:10.1038/s41580-024-00700-8 (2024).

15 Zhang, D. *et al.* Metabolic regulation of gene expression by histone lactylation. *Nature* **574**, 575-580, doi:10.1038/s41586-019-1678-1 (2019).

16 Zong, Z. *et al.* Alanyl-tRNA synthetase, AARS1, is a lactate sensor and lactyltransferase that lactylates p53 and contributes to tumorigenesis. *Cell* **187**, 2375-2392 e2333, doi:10.1016/j.cell.2024.04.002 (2024).

17 Ju, J. *et al.* The alanyl-tRNA synthetase AARS1 moonlights as a lactyltransferase to promote YAP signaling in gastric cancer. *J Clin Invest* **134**, doi:10.1172/JCI174587 (2024).

18 Wang, Y. *et al.* AARS1 promotes tumor progression and immune evasion via ATF6 lactylation-mediated tryptophan metabolism in hepatocellular carcinoma. *Cell Metabolism*, doi:10.1016/j.cmet.2026.06.003.

19 Li, H. *et al.* AARS1 and AARS2 sense L-lactate to regulate cGAS as global lysine lactyltransferases. *Nature*, doi:10.1038/s41586-024-07992-y (2024).

20 Gutierrez, J. A. *et al.* Ghrelin octanoylation mediated by an orphan lipid transferase. *Proc Natl Acad Sci U S A* **105**, 6320-6325, doi:10.1073/pnas.0800708105 (2008).

21 Kojima, M. *et al.* Ghrelin is a growth-hormone-releasing acylated peptide from stomach. *Nature* **402**, 656-660, doi:10.1038/45230 (1999).

22 Yang, J., Brown, M. S., Liang, G., Grishin, N. V. & Goldstein, J. L. Identification of the acyltransferase that octanoylates ghrelin, an appetite-stimulating peptide hormone. *Cell* **132**, 387-396, doi:10.1016/j.cell.2008.01.017 (2008).

23 Zmuda, A. J. *et al.* A universal metabolite repair enzyme removes a strong inhibitor of the TCA cycle. *Nat Commun* **15**, 846, doi:10.1038/s41467-024-45134-0 (2024).

24 Zhang, M. *et al.* A STAT3 palmitoylation cycle promotes TH17 differentiation and colitis. *Nature* **586**, 434-439, doi:10.1038/s41586-020-2799-2 (2020).

25 Yu, Q. *et al.* Sirtuin 5-Mediated Desuccinylation of ALDH2 Alleviates Mitochondrial Oxidative Stress Following Acetaminophen-Induced Acute Liver Injury. *Adv Sci (Weinh)* **11**, e2402710, doi:10.1002/advs.202402710 (2024).

26 Zhao, S., Zhang, X. & Li, H. Beyond histone acetylation-writing and erasing histone acylations. *Curr Opin Struct Biol* **53**, 169-177, doi:10.1016/j.sbi.2018.10.001 (2018).

27 Huang, H. *et al.* Lysine benzoylation is a histone mark regulated by SIRT2. *Nat Commun* **9**, 3374, doi:10.1038/s41467-018-05567-w (2018).

28 Jiang, Y. *et al.* Isonicotinylation is a histone mark induced by the anti-tuberculosis first-line drug isoniazid. *Nat Commun* **12**, 5548, doi:10.1038/s41467-021-25867-y (2021).

29 Xu, M. *et al.* Palmitoyltransferase ZDHHC3 Aggravates Nonalcoholic Steatohepatitis by Targeting S-Palmitoylated IRHOM2. *Adv Sci (Weinh)* **10**, e2302130, doi:10.1002/advs.202302130 (2023).

30 Chang, Y. *et al.* Palmitoylation regulates myelination by modulating the ZDHHC3-Cadm4 axis in the central nervous system. *Signal Transduct Target Ther* **9**, 254, doi:10.1038/s41392-024-01971-5 (2024).

31 Yao, H. *et al.* Inhibiting PD-L1 palmitoylation enhances T-cell immune responses against tumours. *Nat Biomed Eng* **3**, 306-317, doi:10.1038/s41551-019-0375-6 (2019).

32 Zhang, F. *et al.* Deacetylation of MTHFD2 by SIRT4 senses stress signal to inhibit cancer cell growth by remodeling folate metabolism. *J Mol Cell Biol* **14**, doi:10.1093/jmcb/mjac020 (2022).

33 Choi, M. M. *et al.* Identification of ADP-ribosylation site in human glutamate dehydrogenase isozymes. *FEBS Lett* **579**, 4125-4130, doi:10.1016/j.febslet.2005.06.041 (2005).

34 Mathias, R. A. *et al.* Sirtuin 4 is a lipoamidase regulating pyruvate dehydrogenase complex activity. *Cell* **159**, 1615-1625, doi:10.1016/j.cell.2014.11.046 (2014).

35 Gong, X., Feng, Y. & Tang, H. A metabolic labeling protocol to enrich myristoylated proteins from Caenorhabditis elegans. *STAR Protoc* **2**, 101013, doi:10.1016/j.xpro.2021.101013 (2021).

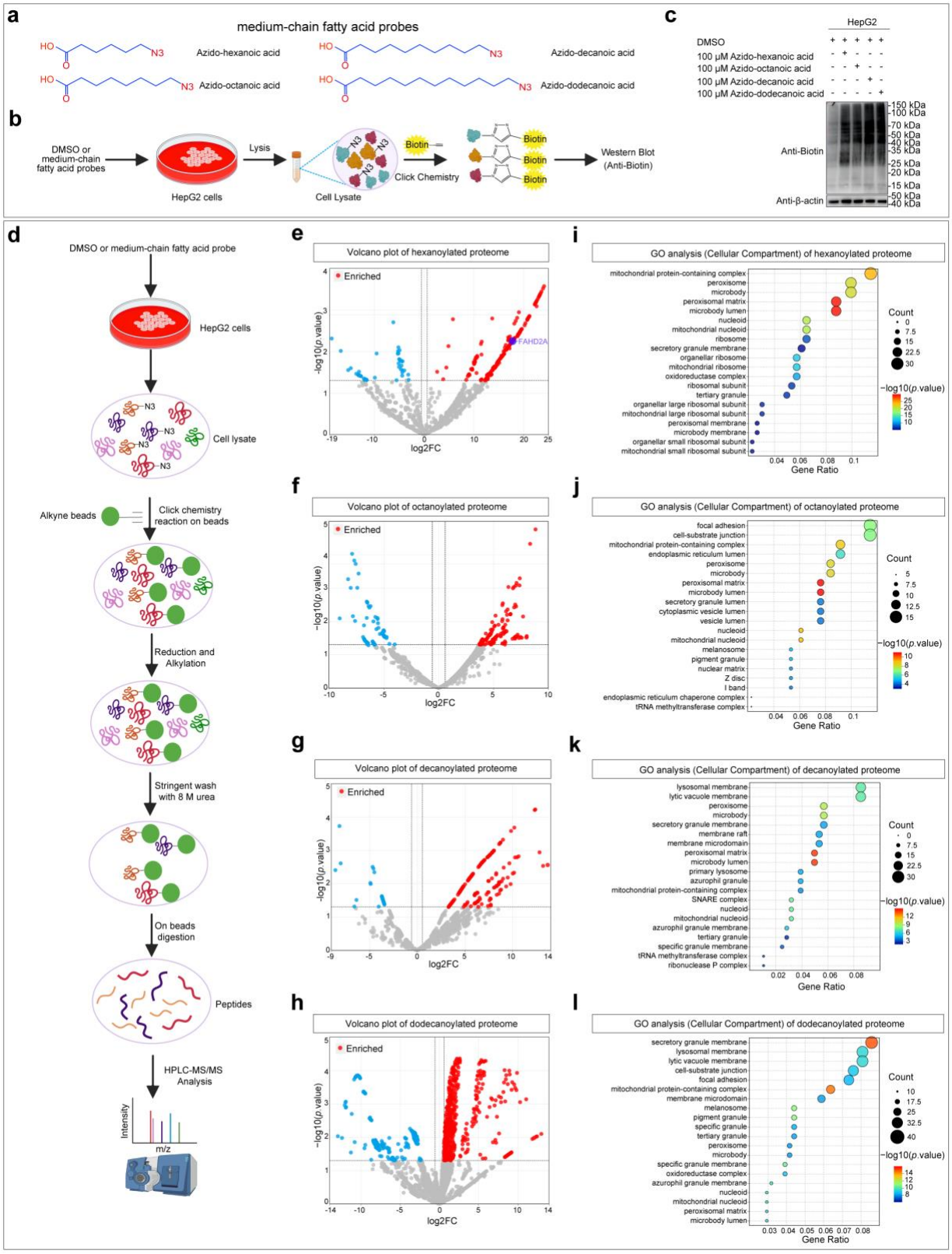

Figure 1. Discovery and profiling of medium-chain acylated proteomes

(a) Chemical structures of the azido MCFA metabolic probes used in this study.

(b) Schematic of the click chemistry-coupled Western blot workflow for detecting global protein acylation, including hexanoylation, octanoylation, decanoylation, and dodecanoylation.

(c) Western blot analysis of global medium-chain acylation levels in HepG2 cells treated for 48 hours with DMSO or 100 μM of the indicated azido-MCFA probes. Biotinylated proteins were detected by anti-Biotin antibody. β-actin serves as a loading control.

(d) Schematic of the chemoproteomic workflow used for the enrichment and identification of medium-chain acylated proteins.

(e-h) Volcano plots displaying proteins enriched from HepG2 cells treated with probes for (e) hexanoylation, (f) octanoylation, (g) decanoylation, and (h) dodecanoylation, relative to DMSO controls. The x-axis represents $\log_2$ (fold change), and the y-axis represents $-\log_{10}$ (p-value). Proteins enriched above the threshold (fold change > 1.5, and $p < 0.05$, dashed lines) are shown in red.

(i-l) Gene Ontology (GO) cellular compartment analysis of significantly enriched proteins from the (e) hexanoylation, (f) octanoylation, (g) decanoylation, and (h) dodecanoylation proteomes.

All experiments were performed with at least three independent biological replicates.

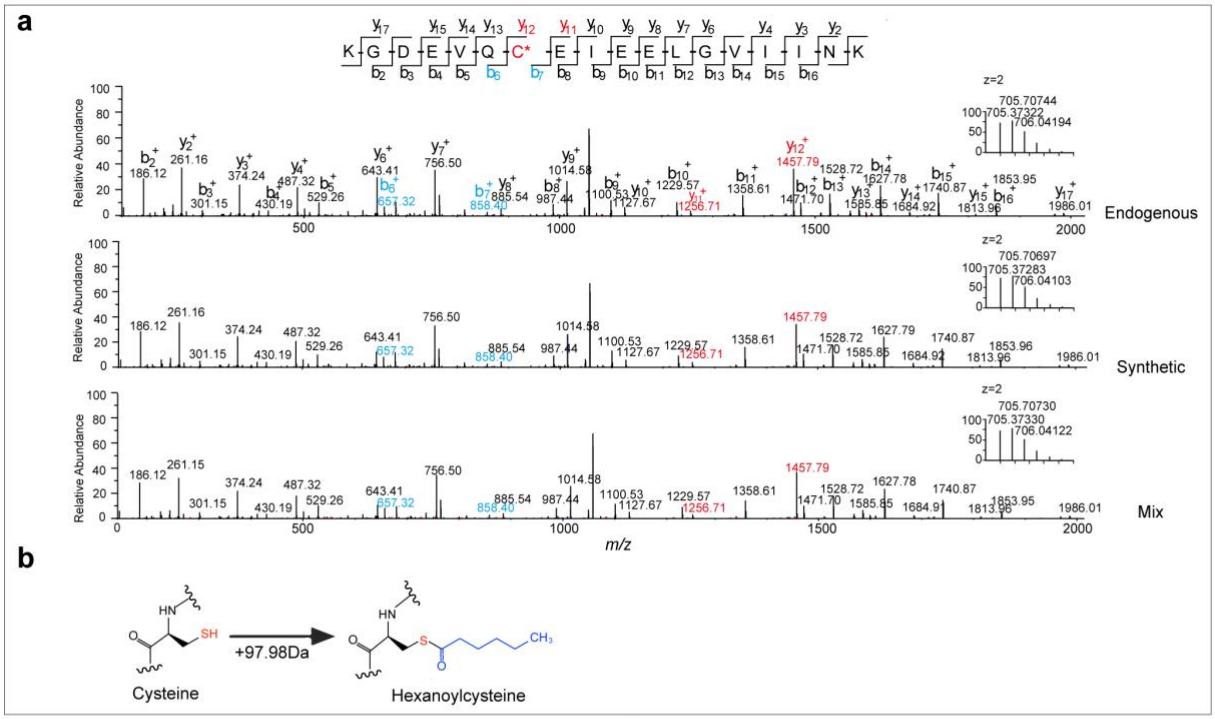

Figure 2. Identification and validation of cysteine hexanoylation on FAHD2A

(a) MS/MS fragmentation spectra of the hexanoylated FAHD2A peptide ($Cys301_{hex}$) derived from FAHD2A-FLAG stably-expressed in HepG2 cells, its synthetic counterpart, and a 1:1 mixture of both. Key b- and y-ions are indicated.

(b) Chemical structure of S-hexanoylcysteine.

(c) Schematic of the workflow for detecting FAHD2A hexanoylation via metabolic labeling, immunoprecipitation, click chemistry and western blot from cells stably expressing FAHD2A-FLAG.

(d) Western blot analysis confirming FAHD2A hexanoylation. HepG2 or 293T cells expressing FAHD2A-FLAG were treated with 100 μM azido-hexanoic acid or hexanoic acid control. Hexanoylation was detected via click chemistry conjugation to biotin, followed by anti-Biotin immunoblotting.

(e) Western blot analysis comparing hexanoylation of wild-type (WT) and C301S mutant FAHD2A tagged with FLAG expressed in HepG2 cells. Experiments were performed as in (c). Biotin immunoblotting reflects FAHD2A hexanoylation levels, while anti-FLAG immunoblotting indicates FAHD2A protein input.

(f) Quantification of relative hexanoylation levels of the C301S mutant compared to wild-type FAHD2A from (e). The FAHD2A hexanoylation was normalized to the total FAHD2A protein level and the hexanoylation level of FAHD2A-WT as the control was set to 1.

All experiments were performed with at least three independent biological replicates. Data are presented as mean ± SEM. Statistical significance was determined by two-tailed unpaired t-test (f).

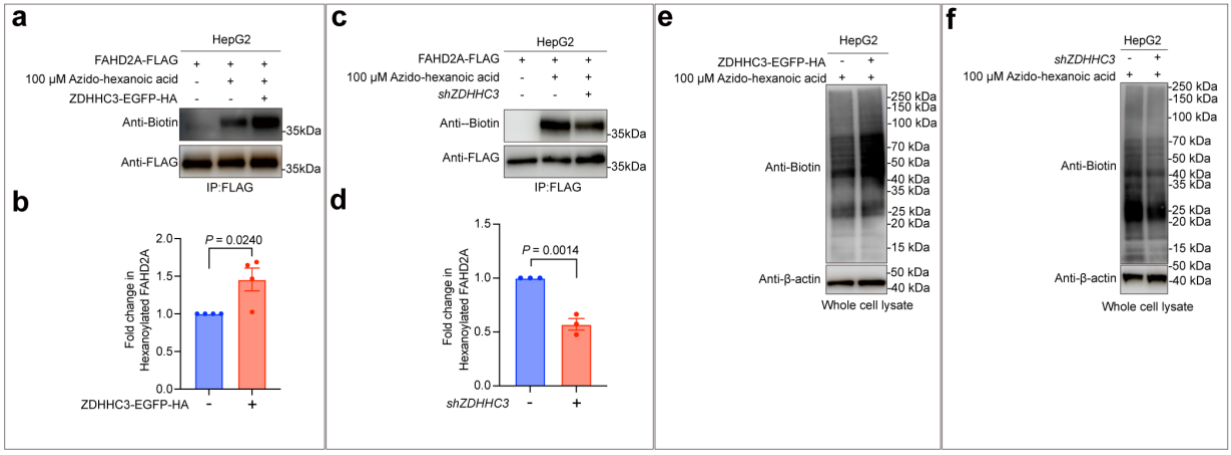

Figure 3. ZDHHC3 is a putative "writer" of protein hexanoylation.

(a, b) Overexpression of ZDHHC3 enhances FAHD2A hexanoylation. (a) Immunoblot analysis of FAHD2A hexanoylation in HepG2 cells expressing FAHD2A-FLAG with or without ZDHHC3-EGFP-HA overexpression. (b) Quantification of relative FAHD2A hexanoylation levels from (a). The FAHD2A hexanoylation level was normalized to the total FAHD2A protein level and the hexanoylation level of control group (with 100 μM azido-hexanoic acid but without ZDHHC3-EGFP-HA overexpression) was set to 1.

(c, d) ZDHHC3 is required for FAHD2A hexanoylation. (c) Immunoblot assessment of FAHD2A hexanoylation in HepG2 cells following *ZDHHC3* knockdown (*shZDHHC3*). (d) Quantification of relative FAHD2A hexanoylation levels from (c). The FAHD2A hexanoylation level was normalized to the total FAHD2A protein level and the hexanoylation level of control group (with 100 μM azido-hexanoic acid but without *shZDHHC3*) was set to 1.

(e) ZDHHC3 overexpression elevates global protein hexanoylation. Immunoblot detection of global protein hexanoylation in HepG2 cells with or without ZDHHC3-EGFP-HA overexpression.

(f) ZDHHC3 is required for global protein hexanoylation. Immunoblot analysis of global protein hexanoylation in HepG2 cells with or without *ZDHHC3* knockdown.

All data are presented as mean ± SEM from at least three independent experiments. Statistical significance was determined by two-tailed unpaired t-test (b, d).

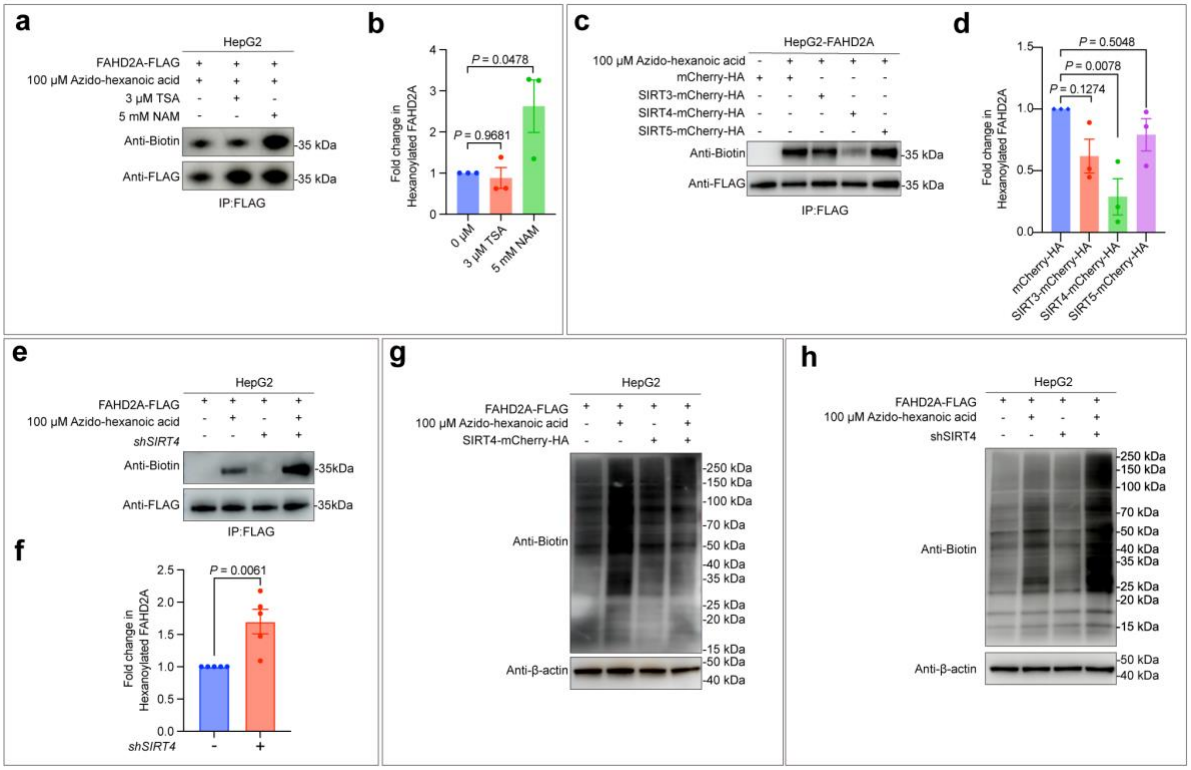

Figure 4. SIRT4 is a potential "eraser" of protein hexanoylation

(a, b) A sirtuin inhibitor increases FAHD2A hexanoylation. (a) Immunoblot of FAHD2A hexanoylation in HepG2 cells treated with the HDAC inhibitor TSA or the SIRT inhibitor NAM. (b) Quantification of relative FAHD2A hexanoylation from (a). The FAHD2A hexanoylation level was normalized to the total FAHD2A protein level and the hexanoylation level of control group (with 100 μM azido-hexanoic acid but without inhibitors) was set to 1.

(c, d) SIRT4 is a potent dehexanoylase for FAHD2A. (c) Immunoblot analysis of FAHD2A hexanoylation in HepG2 cells overexpressing control (mCherry), SIRT3, SIRT4, or SIRT5. (d) Quantification of relative FAHD2A hexanoylation from (c). The FAHD2A hexanoylation level was normalized to the total FAHD2A protein level and the hexanoylation level of control group (with 100 μM azido-hexanoic acid but without SIRT expression) was set to 1.

(e, f) SIRT4 is required to dehexanoylate FAHD2A. (e) Immunoblot of FAHD2A hexanoylation in HepG2 cells following SIRT4 knockdown (*shSIRT4*+) compared to a non-targeting control (*shSIRT4*-). (f) Quantification of relative levels of FAHD2A hexanoylation from (e). The FAHD2A hexanoylation level was normalized to the total FAHD2A protein level and the

hexanoylation level of control group (with 100 μM azido-hexanoic acid but without *shSIRT4*) was set to 1.

(g, h) SIRT4 negatively regulates global protein hexanoylation. Immunoblot of global protein hexanoylation levels in HepG2 cells with SIRT4 overexpression (g) or with SIRT4 knockdown (h).

All data are shown as mean ± SEM from at least three independent experiments. Statistical significance was assessed by one-way ANOVA with Dunnett's multiple comparisons test (d), and two-tailed unpaired t-test (f).

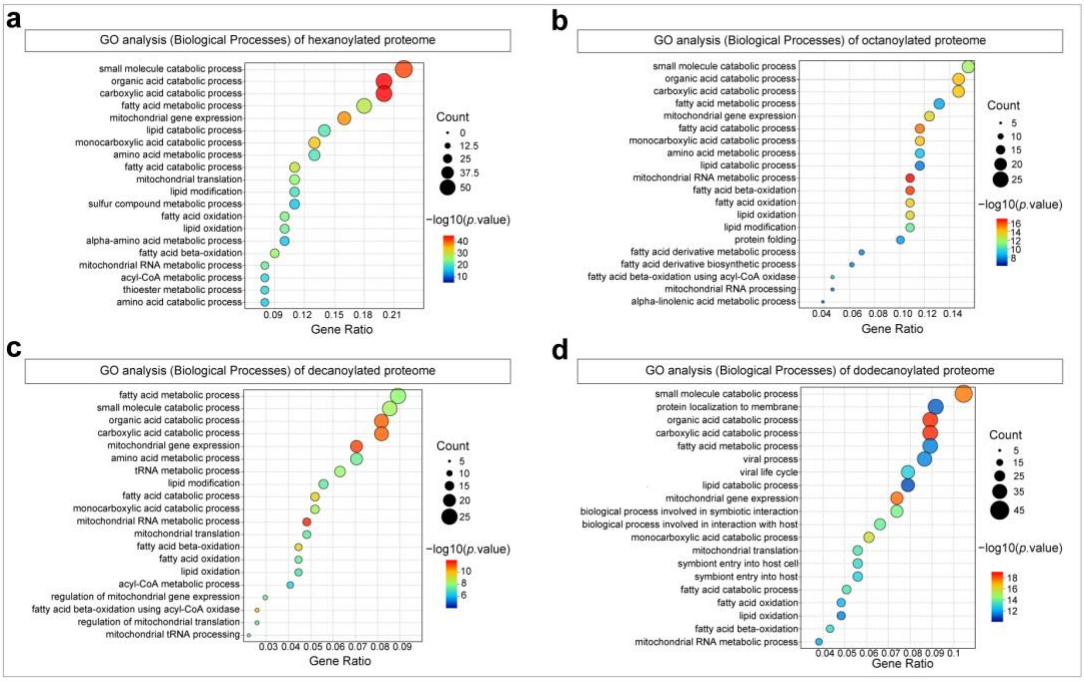

Extended Data Figure 1. Gene Ontology biological process analysis of medium-chain acylomes

(a-d) Gene Ontology (GO) biological process analysis of significantly enriched proteins from the: (e) Hexanoylation proteome, (f) Octanoylation proteome, (g) Decanoylation proteome, and (h) Dodecanoylation proteome in Figure 1. GO terms are ranked by their p-values, with color intensity reflecting the magnitude of $-\log_{10}$ (p-value) for each enriched term.

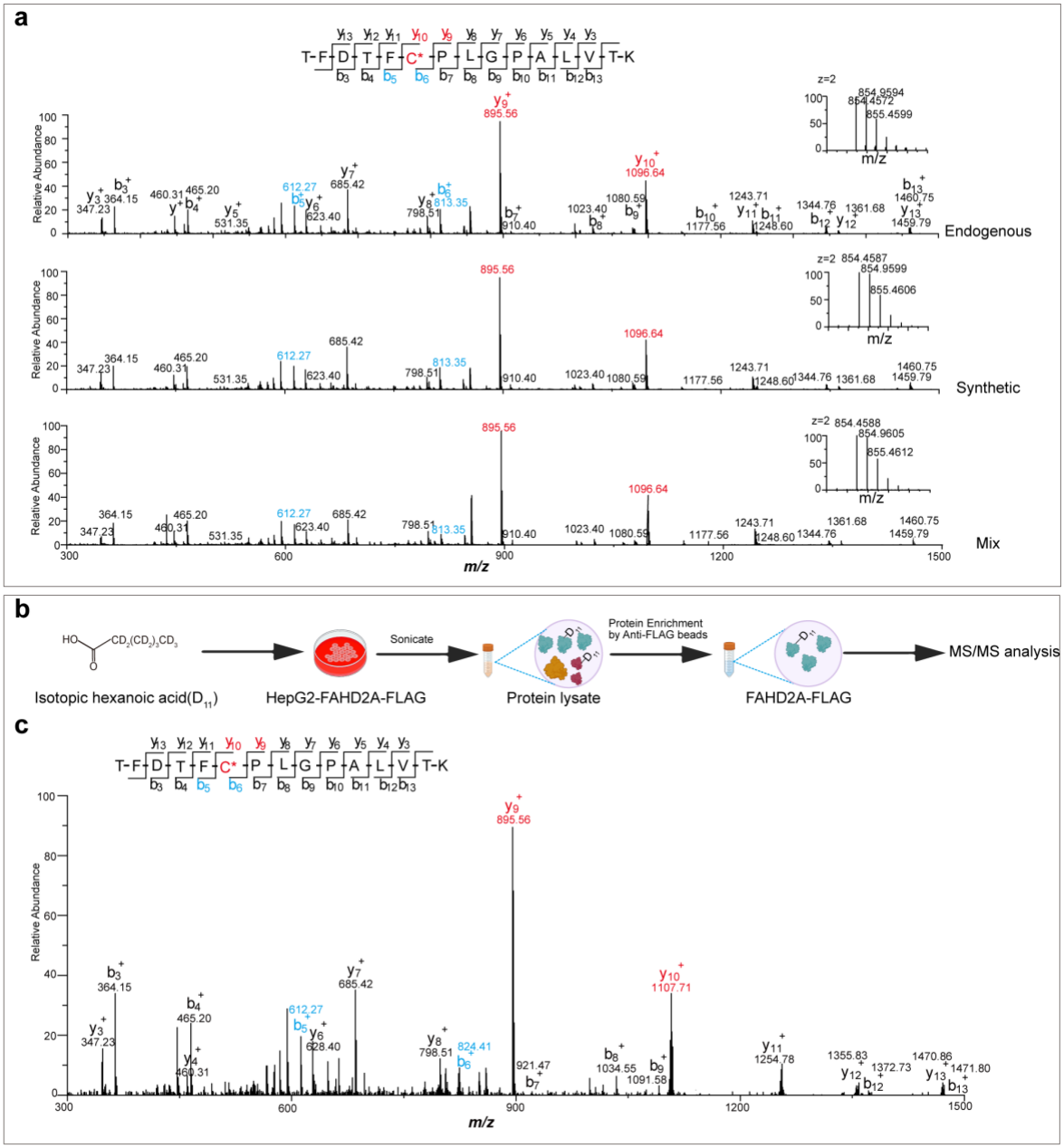

Extended Data Figure 2. Validation of FAHD2A hexanoylation

(a) MS/MS validation of the second hexanoylation site on FAHD2A at Cys215. Fragmentation spectra of the hexanoylated peptide (TFDTFC$_{hex}$PLGPALVTK) derived from endogenously isolated FAHD2A-FLAG in HepG2 cells are compared with its synthetic counterpart and a 1:1 mixture, confirming their identical fragmentation patterns and complementing the data for Cys301 shown in the main figure (Fig. 2a).

626 **(b, c)** Hexanoylation is directly derived from exogenous hexanoic acid. (b) Schematic of the D11-
627 heavy isotope labeling workflow to analyze cysteine hexanoylation of FAHD2A. (c)
628 Representative MS/MS spectrum of a D11-labeled FAHD2A peptide (TFDTFC$_{D11\text{-}hex}$PLGPAL
629 VTK) exhibiting a +109.1422 Da mass shift on cysteine residue, identified in HepG2 cells
630 expressing FAHD2A-FLAG and cultured with D11-hexanoic acid.

631 All spectra shown are representative of results from three independent biological replicates.

632

633

634

635

636

637

638

639

640

641

642

643

644

645

646

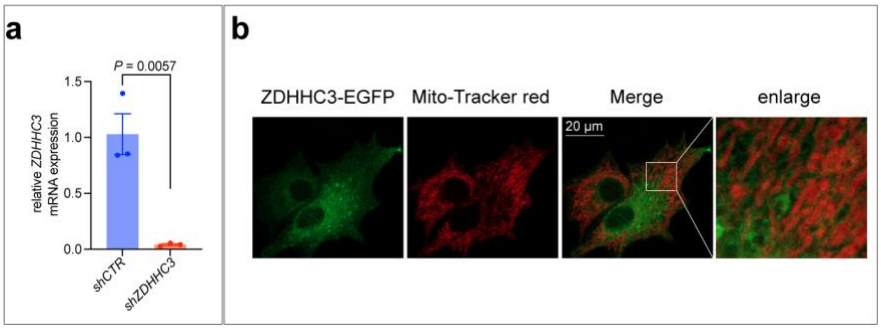

Extended Data Figure 3. Subcellular localization of ZDHHC3 and validation of ZDHHC3 knockdown

(a) qPCR analysis confirming efficient knockdown of *ZDHHC3*. mRNA levels in HepG2 cells expressing shRNA targeting *ZDHHC3* (*shZDHHC3*) were measured relative to a non-targeting control (*shCTR*). Data are presented as mean ± SEM from three independent experiments. Statistical significance was determined by two-tailed unpaired t-test.

(b) Confocal microscopy images show no colocalization between ZDHHC3-EGFP (green) and mitochondria labeled with MitoTracker Red in HepG2 cells. Scale bar: 20 μm.

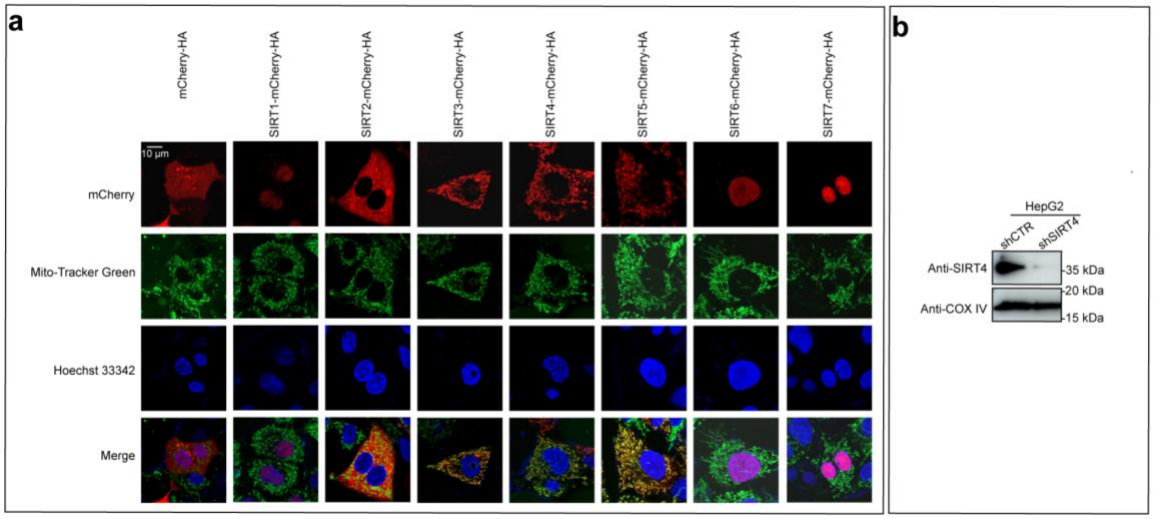

Extended Data Figure 4. Subcellular localization of SIRT family members and validation of SIRT4 knockdown

(a) SIRT3, SIRT4, and SIRT5 localize to mitochondria. Representative confocal microscopy images of HepG2 cells expressing the indicated SIRT-mCherry-HA fusion proteins (red) are shown. Mitochondria were labeled with MitoTracker Green (green), and nuclei were stained with Hoechst 33342 (blue). The merged images confirm the mitochondrial localization of SIRT3, SIRT4, and SIRT5. Scale bar, 10 μm.

(b) Validation of SIRT4 protein knockdown. Immunoblot analysis of SIRT4 protein levels in HepG2 cells expressing a non-targeting control shRNA (*shCTR*) or an shRNA targeting SIRT4 (*shSIRT4*). COX IV serves as a loading control. The immunoblot in (b) is representative of three independent experiments.